ADVANCES IN COASTAL AND OCEAN ENGINEERING

Volume 7

Editor

Philip L.-F. Liu
Cornell University

World Scientific
Singapore • New Jersey • London • Hong Kong

Thorpe, S. A. (1992). Bubble clouds and dynamics of the upper ocean. *Q. J. R. Meteor. Soc.* **118**: 1–22.

Ting, F. C. K. and J. T. Kirby (1995). Dynamics of surf-zone turbulence in a strong plunging breaker. *Coastal Engineering* **24**: 177–204.

Vagle, S. and D. M. Farmer (1998). A comparison of four methods for bubble size and void fraction measurements. *IEEE J. Oceanic Engr.* **23**(3): 211–222.

Vagle, S. and D. M. Farmer (1992). The measurement of bubble-size distribution by acoustical backscatter. *J. Atmos. Ocean. Tech.* **9**: 630–644.

Willert, C. E. and M. Gharif (1991). Digital particle imaging velocimetry. *Exps. Fliuds* **10**: 181–193.

Wood, A. B. (1941). *A Textbook of Sound*, 2nd Edition, G. Bell, London.

Zhang, D. P., T. Sunamura, S. Tanaka and K. Yamamoto (1994). Laboratory experiment of long-shore bars produced by breaker-induced vortex action. *Proc. Coastal Dynamics*, pp. 29–43.

SIMULATION OF WAVES IN HARBORS USING TWO-DIMENSIONAL ELLIPTIC EQUATION MODELS

VIJAY PANCHANG and Z. DEMIRBILEK

Ports and harbors are the center of social, cultural, economic, governmental, military activities and are closely tied to the national economy of the continental United States. Many local and state economies are dependent on waterborne commerce as a major source of transport and enhanced port capacity is vital to Nation's economy, trade and commerce. Several major U.S. ports/harbors currently have renovation plans in response to the expansion of ocean-borne world commerce and coastal engineering projects (dealing with wave agitation in harbors caused by expansion (landfills), channel deepening and widening, flaring channels for improved navigability, channel maintenance and other infrastructure modifications) generally require a detailed knowledge of the wave field in the project areas. Physical and numerical model studies are often conducted concurrently for these projects to evaluate technical feasibility and to optimize design alternatives. This paper provides a comprehensive review of mathematical modeling procedures developed in recent years in the area of elliptic wave equations suitable for simulating waves in ports and harbors. Modeling techniques and extensions of the well-accepted mild-slope wave equation to include steep-slopes, realistic boundary conditions, dissipative mechanisms like friction and breaking, wave-wave and wave-current interactions are discussed. Assumptions such as constant water depths outside the modeling area and fully reflecting exterior coastlines, which plagued earlier elliptic models, have been eliminated in recent treatments of the open boundary. The development of several improved boundary conditions that can be used along coastlines, islands and structures (jetties, breakwaters, etc.) in the modeling domain is discussed. These improvements in the boundary conditions, along with the inclusion of dissipative effects like breaking, allow for more accurate treatment of the scattered and reflected waves throughout the model domain and lead to a realistic representation of waves in complex regions of highly varying bathymetry and boundary types. We describe advances pertaining to the computing efficiency of elliptic wave models which has until recently been a major drawback for these models. Using advanced parallelization schemes, we have been able to reduce the computational time for prototype-scale applications to the order of a few seconds for monochromatic waves and to less than one hour for the simulation of multi-directional irregular sea states. We present a computational framework for including wave-wave and wave-current interactions in elliptic wave modeling. Application of elliptic modeling methods to wave transformation in the Los Angeles/Long Beach Harbor complex and in Barber's Point Harbor are described. Some research areas have been identified.

1. Introduction

Ports and harbors play a vital role in the growth and well-being of many nations. They are important hubs for commercial, military and recreational activities. For instance, about $600 billion in foreign trade passed through ports in the United States in 1997; this trade is projected to triple by 2020 (YOTO, 1998). Engineers must provide the infrastructure that can handle this growth. Harbor facilities must accommodate ever larger ships ("megaships") with increasingly demanding schedules and complex environmental regulations. It is therefore critical that these facilities be designed in a manner that enhances efficiency and safety of harbors operations like cargo loading/unloading, etc.

One of the physical features that can have an adverse impact on harbor operations is the wave climate. For example, some waves (not necessarily big waves) lead to undesirable vessel motions (resulting in operational difficulties such as broken mooring lines, downtime for cargo handling, etc.) or undesirable sediment movement (resulting in more frequent dredging). Reliable estimation of wave conditions in and around a harbor is vital to the success of harbor operations. This estimation must often be accomplished through mathematical modeling techniques. However, most harbors confront the modeler with numerous complexities. Geometrically, as may be seen in Fig. 1, the domain to be modeled may include completely arbitrary coastline shapes and bathymetric features as well as man-made structures like piers, jetties, breakwaters, etc. These features induce wave refraction, diffraction, reflection and dissipation by friction and breaking to varying degrees. The incident waves of interest may cover a wide spectrum, from very short waves to extremely long period waves that cause resonance and may approach the harbor from any direction. For short waves, the number of grids needed to discretize the domain can be extremely large, making the modeling difficult. Longer waves may need fewer grids, but require a better specification of boundary reflectivities since they are more susceptible to reflections in all directions from structures, coastlines, and bathymetric slopes. In addition to these complexities, the modeler may also have to account for the effects of the interaction between various wave components and of tidal or other currents which can magnify or diminish the wave climate in different parts of the domain.

In this paper, we describe a methodology that has become well-accepted in recent years for modeling the situation described above (See Panchang *et al.*, 1999 for a review of recent coastal wave modeling methods). In its basic form, the methodology is based on solving the following two-dimensional

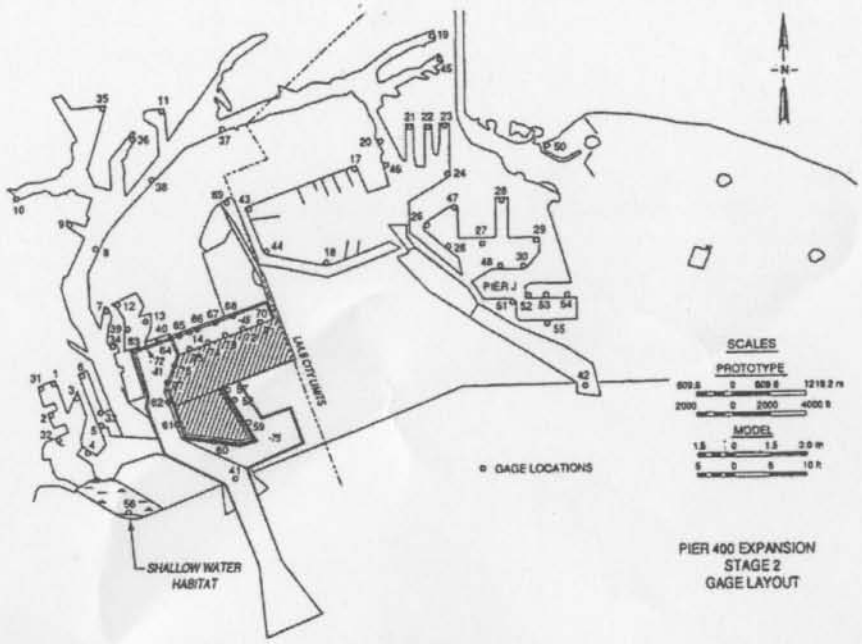

Fig. 1. Los Angeles/Long Beach Harbor area. Numbers show gage locations for hydraulic model study (after Seabergh and Thomas, 1995).

elliptic equation,

$$\nabla \cdot (CC_g \nabla \phi) + k^2 CC_g \phi = 0\,, \tag{1}$$

where,

$\phi(x, y)$ = complex surface elevation function $(= \phi_1 + i\phi_2)$

$i = \sqrt{-1}$

σ = wave frequency under consideration

$C(x, y)$ = phase velocity $= \sigma/k$

$C_g(x, y)$ = group velocity $= \partial\sigma/\partial k$

$k(x, y)$ = wavenumber $(= 2\pi/L)$ related to the local depth $d(x, y)$ through the dispersion relation,

$$\sigma^2 = gk \tanh(kd)\,. \tag{2}$$

The wave height H can be obtained from complex surface elevation function ϕ as follows,

$$H = \frac{2\sigma}{g}\sqrt{(\phi_1^2 + \phi_2^2)}\,. \tag{3}$$

Essentially Eq. (1) represents an integration over the water column of three-dimensional Laplace equation used in potential wave theory. The integration, originally described by Berkhoff (1976) and Smith and Sprinks (1975), is necessary because the solution of the three-dimensional problem is computationally difficult for harbors with a characteristic length that is several times of the wavelength. The integration is based on the assumption that the vertical variation of the wave potential is largely the same as that for a horizontal bottom, i.e.,

$$\varphi(x, y, z) \approx \frac{\cosh k(d+z)}{\cosh kd}\phi(x, y)\,. \tag{4}$$

This approximation is obviously valid for a "mild slope" characterized by $|\nabla d|/kd \ll 1$, a criterion that is usually met in practice (extensions to steep slopes are described later). Being elliptic, Eq. (1) represents a boundary value problem which can accommodate internal nonhomogeneities. It hence forms a widely-used basis for performing wave simulations in regions with arbitrarily-shaped (manmade or natural) boundaries and arbitrary depth variations. Unlike "approximate" mild slope wave models (e.g., REFDIF and RCPWAVE described by Dalrymple *et al.*, 1984; Kirby, 1986; Ebersole, 1985), there are no intrinsic limitations on the shape of the domain, the angle of wave incidence, or the degree and direction of wave reflection and scattering that can be modeled with Eq. (1). In essence, Eq. (1) represents the complete two-dimensional wave scattering problem for the nonhomogeneous Helmholtz equation as demonstrated by Radder (1979). While it is valid for a monochromatic (single incident frequency-direction) wave condition, irregular wave conditions may be simulated using Eq. (1) by superposition of monochromatic simulations.

For further development in this paper, we may consider the following extended form of Eq. (1),

$$\nabla \cdot (CC_g \nabla\phi) + (k^2 CC_g + iC_g\sigma W)\phi = 0\,, \tag{5}$$

in which a dissipation term W has been included. By separating the real and imaginary parts of Eq. (5), Booij (1981) has shown that Eq. (5) satisfies the energy balance equation in the presence of dissipation. The term W may represent breaking and/or friction and is described later.

Several computational models based on Eq. (1) or Eq. (5) have been developed in recent years. These models differ in the choice of the numerical method used (e.g., finite-difference method, boundary element method, finite element method), in the choice of boundary conditions, in the method used to solve the linear system of equations that results from discretizing the elliptical governing equation, and in the inclusion of additional mechanisms. In this paper, we provide a review of the modeling techniques pertaining to the application of Eq. (1) to harbors. The layout of this paper is as follows. Sections 2 and 3 describe the various kinds of boundary conditions and numerical solution methods that have been developed in recent years. Section 4 describes the incorporation of additional mechanisms in Eq. (5). The application of a comprehensive finite-element model to simulate waves in the Los Angeles/Long Beach harbor complex (Fig. 1) and in Barber's Point Harbor is described in Sec. 5.

2. Boundary Conditions

Domains on which the elliptic equation Eq. (5) is solved are enclosed by closed boundaries (represented by coastlines and surface-penetrating structures like pier walls or pier legs, breakwaters, seawalls, etc.) and open boundaries (which represent an artificial boundary between the area being modeled and the sea region outside). A separation between the model domain and an outer water area from where no waves enter the model domain (e.g., a creek or tributary at the backbay or down wave end of the domain) may be considered to be a fully-absorbing closed boundary. An open boundary is considered to be the one where an incident wave is specified (and may contain other radiated waves). Along all boundaries, appropriate conditions must be specified to solve Eq. (1); however, even in the best of circumstances, only approximate boundary conditions can be developed (e.g., see Dingemaans, 1997).

2.1. *Closed boundary conditions*

Along coastline and surface-protruding structures, the following boundary condition has traditionally been used (e.g., Berkhoff, 1976; Tsay and Liu, 1983; Tsay *et al.*, 1989; Oliveira and Anastasiou, 1998; Li, 1994a),

$$\frac{\partial\phi}{\partial n} = \alpha\phi\,, \tag{6}$$

where n is the outward normal to the boundary and α is related to a user-specified reflection coefficient as follows,

$$\alpha = ik\frac{1-K_r}{1+K_r}. \tag{7}$$

K_r varies between 0 and 1 and specific values for different types of reflecting surfaces have been compiled by Thompson *et al.* (1996).

It may be verified that Eq. (6) is strictly valid only for fully-reflecting boundaries (i.e., $K_r = 1$). For partially reflecting boundaries, it is valid only if waves approach the boundary normally. For other conditions, Eq. (6) is approximate and may produce distortions in the model solutions. These limitations may be eliminated by describing the solution at the boundary more fully as a sum of incident and reflected waves,

$$\phi = A\{\exp[ik(n\cos\theta + s\sin\theta)] + K_r\exp[ik(-n\cos\theta + s\sin\theta + \beta)]\}, \tag{8}$$

where A is the amplitude of the approaching waves, θ is the direction at which they intersect the boundary ($\theta = 0$ for normally incident waves), s is the coordinate along the tangent to the boundary, and β is a phase shift between the incident and the reflected wave. Equation (8) leads to the following boundary condition,

$$\frac{\partial\phi}{\partial n} = ik\cos\theta\frac{1-K_r\exp(ik\beta)}{1+K_r\exp(ik\beta)}\phi. \tag{9}$$

Unfortunately, θ and β are not known *a priori* inside the model domain and must be estimated by approximation. For fully absorbing boundaries ($K_r = 0$), Li and Anastasiou (1992) and Li *et al.* (1993) have used Eq. (9) after estimating θ from Snell's Law and the deep-water incident wave angle. Alternatively, Isaacson and Qu (1990) estimated θ as follows,

$$\theta = \arctan\{(\partial\chi/\partial s)/(\partial\chi/\partial n)\}, \tag{10}$$

where χ is the argument of the complex quantity ϕ (i.e., the phase of ϕ). For implementation, they first used Eq. (6) as a boundary condition, obtained χ from the results, determined θ from Eq. (10), used Eq. (9) as a boundary condition to perform a second iteration of the model, recalculated χ and θ, performed a third model iteration using Eq. (9) and so on. Like Pos (1985), they assumed $\beta = 0$ while using Eq. (9), based on limited numerical tests that showed little sensitivity to β. Clearly, like the Snell's Law approach, Eq. (10) is valid only for $K_r = 0$ (although problems with nonzero K_r were also considered). To include the effect of the reflected waves (i.e., the second term in the right hand side of Eq. (8)), Isaacson *et al.* (1993) suggested estimating θ as follows,

$$\theta = (1/k)\arcsin\{\partial\chi/\partial s\}. \tag{11}$$

Again, an iterative method with repeated model calculations were needed. Steward and Panchang (2000) analyzed these methods and noted difficulties with convergence of the above iterative methods and with the quality of the solutions obtained with Eqs. (10) and (11). They were able to eliminate these difficulties by estimating θ from the following expression,

$$\tan\theta = \frac{\partial\chi}{\partial s}\Big/\left(\frac{\partial\chi}{\partial n} + \frac{2K_rk(\cos(k\beta)+K_r)}{1+2K_r\cos(k\beta)+K_r^2}\cos(\theta)\right). \tag{12}$$

Equation (12) is a generalization of Eq. (10) that allows nonzero K_r and β. For a detailed comparison of results, see Steward and Panchang (2000). As an example, Fig. 2 shows a simulation of waves propagating into a rectangular harbor area obtained with Eq. (12). Unlike the results demonstrated by Steward and Panchang (2000) and by Beltrami *et al.* (2000) using other boundary conditions, Fig. 2 contains no spurious oscillations or noise.

Despite the increasing sophistication seen progressively in Eqs. (6) and (9) and in the various ways of estimating θ, some fundamental problems remain. The most important one is inherent in Eq. (8), i.e., the assumption that the total wave field near the boundary can be represented either by one set of plane waves (in the case of Eq. (10) or the Snell's Law approach of Li *et al.* (1993)) or by two sets of plane waves (in the case of Eqs. (11) and (12)) propagating in constant depth. In domains of complex shapes (as in Fig. 1) with arbitrary bathymetry and boundaries with varying reflectivities, a complex pattern of waves can result; simple wave trains are not easily discernible and, as noted by Isaacson and Qu (1990), the definition of a single θ (and β) can become meaningless. Further, even when there is a well-defined train of waves near the boundary (justifying the use of the above methods), precise estimation of K_r and β is still problematic. Values of K_r provided by Thompson *et al.* (1996) certainly do not cover full range of reflecting surfaces that the modeler encounters, nor do they cover the dependence of these parameters on the incident wave frequency. Efforts to incorporate the work of Dickson *et al.* (1995) and Sutherland and O'Donoghue (1998) pertaining to β in models such as the one described here are lacking. In some ways, it may be best to

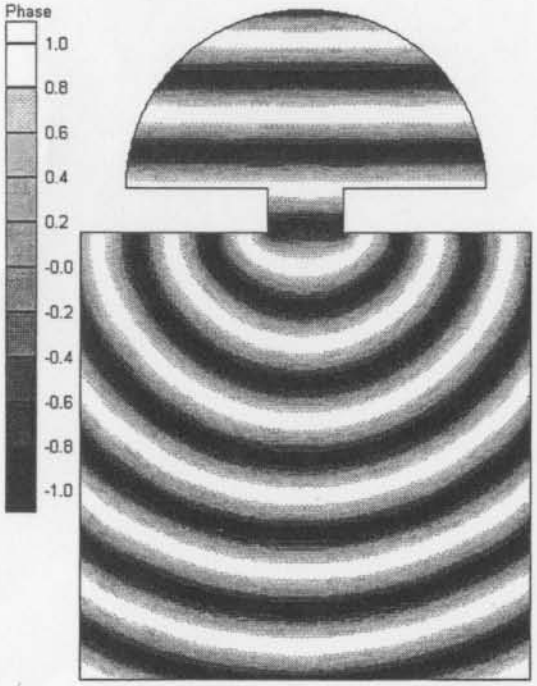

Fig. 2. Modeled waves in a rectangular harbor, using Eqs. (9) and (12). Phase diagram (shows cosine of phase angle). Semicircle represents open boundary. $K_r = 0$ on closed boundaries.

recognize these difficulties at the outset and use the simplest expression of Eq. (6) by combining all the uncertainties noted above into a single parameter α which may be regarded as a tuning parameter.

2.2. *Open boundary conditions*

Along the open boundary, an incident wave ϕ_i must be specified. Along this boundary, however, waves backscattered from within the domain will also exist and their magnitude is generally not known. In the context of simple rectangular domain models with one side (aligned, say, in the y direction) constituting the open boundary, Panchang *et al.* (1988, 1991), Li (1994a, 1994b), and Oliveira and Anastasiou (1998) have used the following condition,

$$\frac{\partial \phi}{\partial x} = ik(2\phi_i - \phi)\,. \tag{13}$$

Equation (13) is obtained by assuming that the incident and backscattered components along this boundary can be described by $\phi_i = A_i \exp(ikx)$ and $\phi_b = \mathrm{B}\exp(-ikx)$ respectively (where A_i is the (specified) amplitude of the incoming wave and B is an unknown), adding the two components and differentiating. Obviously, this is valid only if the incident and backscattered waves near the boundary are plane waves propagating in the $+/-x$ direction.

For more complex domains involving multidirectional scattering, Eq. (13) is inappropriate. Harbor applications generally use model domains such as that described in Fig. 3 where the semicircle is used to separate the model area from the open sea. In the exterior domain Ω', the potential ϕ is comprised of three components,

$$\phi = \phi_i + \phi_r + \phi_s\,, \tag{14}$$

where ϕ_i = the incident wave that must be specified to force the model, ϕ_r = a reflected wave that would exist in the absence of the harbor and

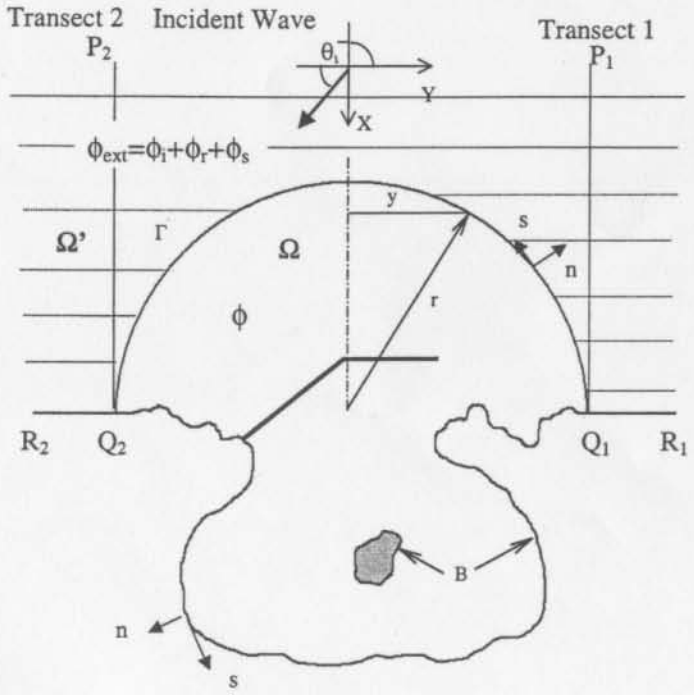

Fig. 3. Harbor wave model domain; definition sketch.

ϕ_s = a scattered wave that emanates as a consequence of the harbor and must satisfy the Sommerfeld radiation condition. With appropriate descriptions for these components, a boundary condition can be developed along the semicircle.

In traditional harbor models (Mei, 1983; Tsay and Liu, 1983; Thompson *et al.*, 1996; Chen and Houston, 1987; Xu and Panchang, 1993; Demirbilek and Panchang, 1998), the exterior wave conditions are described as follows,

$$\phi_i = A_i \exp[ikr\cos(\theta - \theta_i)]\,, \text{ which is the specified input,} \tag{15}$$

$$\phi_r = A_i \exp[ikr\cos(\theta + \theta_i)]\,, \tag{16}$$

$$\phi_s = \sum_{n=0}^{\infty} H_n(kr)(A_n \cos n\theta + B_n \sin n\theta)\,, \tag{17}$$

where (r, θ) denotes the location of a point in polar coordinates, H_n is the Hankel function of the first kind and order n, and A_n and B_n are unknown coefficients.

For the specified incident wave field given by Eq. (15), Eqs. (16) and (17) result from the solution of the relevant eigenvalue problem in the traditional method. As demonstrated by Xu *et al.* (1996), however, this eigenvalue problem in which ϕ_s and ϕ_r are coupled, may be solved only under the following conditions,

(i) the exterior region must have a constant depth,
(ii) the exterior coastlines Q_1R_1 and Q_2R_2 must be fully reflecting and collinear.

These requirements usually cannot be met in practice where the exterior geometry varies arbitrarily and the unrealistic bathymetric representation used by the modeler invariably has an adverse influence on the solution. In field applications, the exterior bathymetry is irregular and the depth generally increases in the offshore-direction. Condition (i) is thus violated, causing two problems as demonstrated by Panchang *et al.* (2000). First, the modeler must arbitrarily select a representative "constant" depth and test the sensitivity of the solutions to these depths. This can be extremely time-consuming. Second, the effect of reflections from the sloping exterior bathymetry is ignored. These effects are often significant especially for long periods that are of interest in harbor resonance studies. Condition (ii) is also problematic. Exterior coastlines are not always fully reflecting for all wave conditions and imposing full reflection in such cases yields extremely large amplification factors and

rapid variations in the wave pattern in the outer regions of the domain. (See examples in Xu *et al.* (1996), Demirbilek *et al.* (1996) and in Thompson *et al.* (1996)). One may of course enlarge the interior region in the hope that these effects do not contaminate the results in the area of interest, however, there is no guarantee that these effects are confined to specific regions. In addition, the extra memory requirements and grid-generation for a larger domain are usually exceedingly demanding. Thus, while Eqs. (16) and (17) constitute rigorous solutions of the eigenvalue problem, their use renders the application of harbor wave models problematic in practice. (One consequence of the above is that many of the models in this category cannot correctly simulate fairly simple phenomena like waves approaching a sloping beach. Investing confidence in model results when applied to field situations is therefore difficult).

To overcome these difficulties, Panchang *et al.* (1993) have described a procedure that requires the exterior domain to be suitably divided into a finite number of regions of constant depths. A boundary integral equation is then developed for each of these exterior regions using the appropriate Green's function. The boundary element formulations for these regions are then matched with each other along the interfaces and with a finite-element network in the model interior to obtain the solution. It was found, however, that this type of model is extremely cumbersome to code and construct for general implementation. Other difficulties may also be expected if mechanisms such as dissipation, wave-current interaction, etc., are to be introduced into the governing equation. Chen (1990) also has suggested discretizing the exterior domain into a finite number of radial "infinite elements" with a prespecified shape function in each element. However, this shape function is entirely dependent on the farfield approximation for the Hankel functions, suggesting that a fairly large computational domain is still needed.

An effective alternative is to use a "parabolic approximation" to describe ϕ_s,

$$\frac{\partial \phi_s}{\partial n} = -p\phi_s - q\frac{\partial^2 \phi_s}{\partial \theta^2}\,, \tag{18}$$

where,

$$p = -ik_0 + \frac{1}{2r} - \frac{i}{8k_0 r^2}\,, \quad q = -\frac{i}{2k_0 r^2}\,, \tag{18a}$$

where r and θ represent the polar coordinates of a point on the open boundary and k_0 is a representative wavenumber for the open boundary (p and q are not unique and alternative forms, each obtained with an appropriate rationale, have been investigated by Givoli (1991), Xu *et al.* (1996), Panchang

et al. (2000)). The parabolic approximation, Eq. (18), allows the scattered waves to exit only through a limited aperture around the radial direction. Unlike Eq. (17), it does not rigorously satisfy the Sommerfeld radiation condition. However, using this formulation decouples ϕ_s from the other components. These components (ϕ_i and ϕ_r) may be obtained by making a compromise between a detailed exterior bathymetric representation (which as noted earlier, is difficult) and the constant depth representation (which is unrealistic). A one-dimensional representation where the depths vary in the cross-shore direction only (Figs. 3 and 4) may be selected. This is reasonable since, in general, this is often the direction in which the depths vary the most. If natural variations do not permit the representation of the exterior depths by only one section, a second one-dimensional section shown as transect 2 in Figs. 3 and 4 may be constructed. For transects 1 and 2 with varying depths, no simple analytical expression (such as Eq. (16)) can be found for the reflected wave (since ϕ_i and ϕ_r are coupled). However, the quantity,

$$\phi_0 = \phi_i + \phi_r\,, \tag{19}$$

may be obtained by the solution of the one-dimensional version of Eq. (5) since the depths along these transects vary in one direction only. This

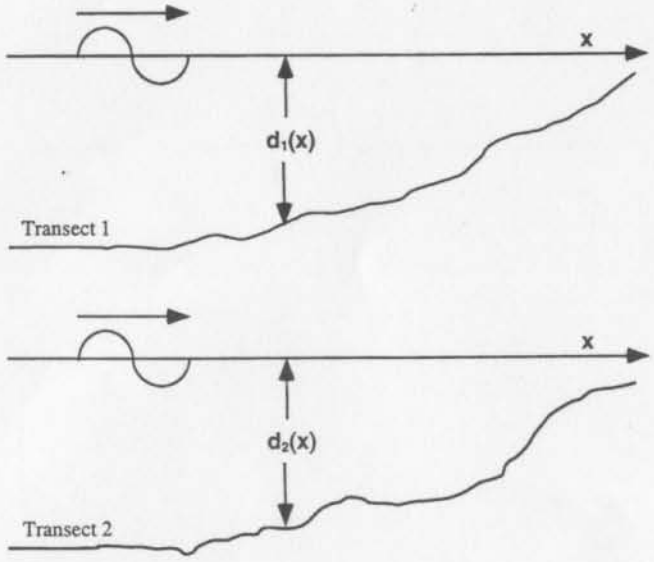

Fig. 4. Two 1D transects representing the exterior bathymetry (do not have to be identical).

one-dimensional equation is (Schaffer and Jonsson, 1992; Panchang *et al.*, 2000),

$$\frac{d}{dx}\left(CC_g\frac{d\psi}{dx}\right) + kCC_g(k\cos^2\theta + iW)\psi = 0\,, \tag{20}$$

where, for one-dimensional geometry,

$$\phi_0 = \psi(x)\exp(iky\sin\theta)\,. \tag{21}$$

Equation (21) is an elliptic ordinary differential equation requiring two boundary conditions. It may easily be solved via a simple finite-difference scheme (for the present, the dissipation factor W is considered to be prespecified). Assuming that transect 1 extends out to a region of constant depth (or deep water), a condition at P_1 may be obtained by combining a specified incident wave,

$$\phi_i(P_1) = A_i\exp(ikx\cos\theta_i + iky\sin\theta_i)\,, \tag{22}$$

(where $A_i = a$ given input wave amplitude) and an unknown reflected wave,

$$\phi_r(P_1) = B\exp(-ikx\cos\theta_i + iky\sin\theta_i)\,. \tag{23}$$

Without loss of generality, the point P_1 may be located at $x = 0$ which allows elimination of B to yield,

$$\frac{\partial\psi}{\partial x} = ik\cos\theta_i(2A_i - \psi)\,. \tag{24}$$

At the coastal boundary point Q_1, the partial reflection boundary condition of Eq. (9) may be used in the following form,

$$\frac{\partial\psi}{\partial x} = \frac{i\sqrt{k^2 - k^2\sin^2\theta}(1 - K_r)}{1 + K_r}\psi\,, \tag{25}$$

where K_r is the reflection coefficient for the exterior coastline (i.e., near Q_1), and $k\sin\theta$ is constant for one-dimensional problem.

The solution of Eq. (20) using boundary conditions, Eqs. (24) and (25), along with Eq. (21) produces ϕ_0 along transects 1 and 2. These solutions are denoted by ϕ_{01} and ϕ_{02}. The desired ϕ_0 along the semicircle may be obtained by laterally translating ϕ_{01} and ϕ_{02} via interpolation between transects 1 and 2 as follows,

$$\phi_0 = (1 - m)\phi_{01}\exp(-ik(r - y)\sin\theta) + m\phi_{02}\exp(ik(r + y)\sin\theta)\,, \tag{26}$$

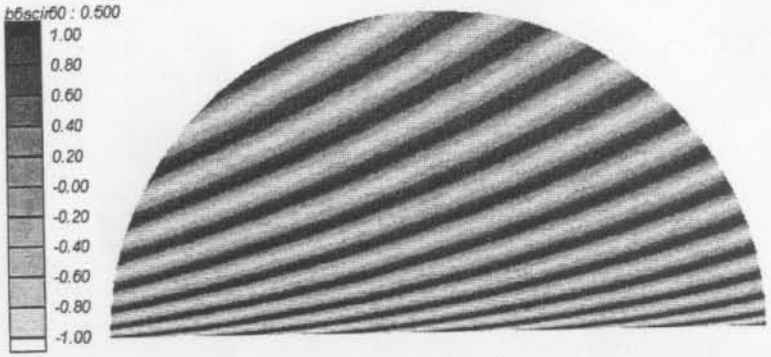

Fig. 5. Modeled wave refraction on a sloping beach; angle of incidence 60°. Phase diagram.

where we have set $y = 0$ at the center of semicircle, the interpolation function $m = (r - y)/2r$, r is the radius of the semicircle, y is the lateral coordinate of the open boundary node relative to the origin of semicircle (Fig. 3).

The boundary condition for ϕ along the semicircle Γ may be obtained by using the continuity of the potential (Eqs. (14) and (19)) and its derivative along with Eqs. (18) and (26),

$$\frac{\partial \phi}{\partial n} = \frac{\partial \phi_0}{\partial n} - p(\phi - \phi_0) - q\frac{\partial^2 \phi}{\partial \theta^2} \,. \tag{27}$$

Thus, the solution of Eq. (20) provides ϕ_0 along the one-dimensional transects. These values can be translated laterally and substituted into Eq. (27) to obtain the open boundary condition for the two-dimensional equation of Eq. (1). Zhao *et al.* (2000) and Panchang *et al.* (2000) have demonstrated that this procedure provides extremely satisfactory solutions for a large number of test cases. An example of wave refraction along a sloping beach is shown in Fig. 5. The expected bending of the crests can be observed with no spurious effects.

3. Numerical Solution

Equation (5) is generally solved using the boundary element method, the finite-difference method, or the finite element method. In general, finite-difference discretizations are not well-suited to represent the complex domain shapes described, for example, in Fig. 1. Not only are the boundaries distorted, but the number of uniformly spaced grids may also be excessively large (adequate resolution, typically 10 points per wavelength, demands that the spacing be determined from the smallest wavelength). Most studies with the finite-difference method have been limited to largely rectangular domains (e.g., Li, 1994a, 1994b; Panchang *et al.*, 1991; Li and Anastasiou, 1992). Boundary element models can handle arbitrary shapes and require minimal storage since only the boundaries are discretized; however, they are limited to subdomains with constant depths only (e.g., Isaacson and Qu, 1990; Lee and Raichlen, 1972; Lennon *et al.*, 1982). Finite element models, on the other hand, allow the construction of grids with variable sizes (based on the local wavelength) and give a good reproduction of the boundary shapes. Most finite element models (e.g., Tsay and Liu, 1983; Tsay *et al.*, 1989; Kostense *et al.*, 1988; Demirbilek and Panchang, 1998; Panchang *et al.*, 2000) have used triangular elements, and modern graphical grid generating software permits efficient and accurate representation of harbors with complex shapes. For example, the Surface Water Modeling System described by Zundell *et al.* (1998) and Jones and Richards (1992) can be used to conveniently generate as many as 500,000 elements of varying size, based on the desired (user-specified) resolution, and to specify the desired reflection coefficients on various segments of the closed boundary. The solution of Eq. (1) by the finite element method is described in detail by Mei (1983) and by Demirbilek and Panchang (1998) when different types of open boundary conditions are used.

Whether one uses finite differences or finite elements for discretization, the numerical treatment of Eq. (1) with appropriately chosen boundary conditions leads to system of linear equations,

$$[\mathrm{A}][\phi] = [\mathrm{B}] \,, \tag{28}$$

where $[\phi]$ represents the vector of all the unknown potentials. For solving Eq. (5), a similar system results as long as W is prespecified. The matrix [A] is usually extremely large. In earlier models (e.g., Tsay and Liu, 1983; Tsay *et al.*, 1989; Chen, 1990; Chen and Houston, 1987), the solution of Eq. (28) was accomplished by Gaussian Elimination which requires enormous memory and is prohibitive when the number of wavelengths in the domain is large (i.e., short waves or a large domain). Pos and Kilner (1987) were able to alleviate this difficulty somewhat by using the frontal solution method of Irons (1970).

In recent years, the solution of Eq. (28) has been obtained with minimal storage requirements for [A]. This is due to the development by Panchang *et al.* (1991) and Li (1994a) of iterative techniques especially suited for Eq. (1). These techniques, based on the conjugate gradient method, guarantee convergence and have been found to be extremely robust in a wide variety

of applications involving both finite differences and finite elements for several kinds of boundary conditions. Hurdle *et al.* (1989) have used the biconjugate gradient algorithm. This variation is efficient when it works but (as noted by Kostense *et al.*, 1997) it does not guarantee convergence for this type of governing equation. More recently, Oliveira and Anastasiou (1998) explored the use of the Generalized Minimum Residual method and the Stabilized Biconjugate Gradient method and reported greater efficiency with finite-difference models based on Eq. (1). With a finite-element formulation, however, Zhao *et al.* (2000) found that the GMRES method of Oliveira and Anastasiou (1998) failed to converge whereas their latter method yielded erratic efficiency.

Alternative solution techniques have also been explored by Li and Anastasiou (1992) who first express ϕ as $\exp(\mu)$ and obtain a new equation for μ. Since μ is sometimes a less rapidly varying function than ϕ, Li and Anastasiou (1992) suggest that as few as 2 or 3 grid points per wavelength will suffice. However, as noted by Li and Anastasiou (1992) and by Radder (1992), the presence of rapidly varying topography or of reflections in various directions will necessitate much finer resolution (say 10 points per wavelength) and the solution obtained by using the log of the potential may lead to excessive smoothing. For mildly varying bathymetry with low reflections, it may in any case be more efficient to solve instead of the "parabolic approximation" of Eq. (1) which is intended for such applications. Li and Anastasiou (1992) have used the multigrid method to minimize storage problems. When higher resolution is required, though, this method does not offer any significant advantage over the conjugate gradient schemes described by Li (1994a) and Panchang *et al.* (1991) since at least one grid with the desired resolution must be constructed. Further, the multigrid method is best suited to rectangular finite-difference discretizations.

Another method, proposed by Li (1994b), involves solving the following parabolic equation,

$$a\frac{d\phi}{dt} = \nabla \cdot (CC_g \nabla \phi) + k^2 CC_g \phi \,, \tag{29}$$

where a is a constant. Equation (29) is an approximation of the time-dependent hyperbolic wave equation associated with Eq. (1). It is solved by marching forward in time until steady state is reached. Equation (29) is similar to the heat equation and standard techniques (e.g., the ADI method) for solving such equations are used by Li (1994b). It must be noted, though, that the elimination

of storage difficulties associated with the elliptic equation as Eq. (1) by (artificially) parabolizing it (as Eq. (29)) is comparable to the iterative methods of solving the elliptic version. The solution obtained at various "timesteps" in the case of Eq. (29) is analogous to the various "iterates" obtained in the quest for convergence in the case of Eq. (1). In fact, marching the unsteady-state heat equation by the basic explicit finite-difference scheme results in values at each timestep that are identical to successive iterates if the elliptic Laplace equation is solved by Jacobi iteration [for more details see Marchuk (1975) and Smith (1978)].

For modeling spectral wave conditions, the input spectrum is discretized into several components and each component is modeled by methods described above. The solution of (or significant wave height) any grid point is calculated by linear superposition (e.g., Li *et al.*, 1993). Significant improvements in speed may be obtained by using two-level code parallelization for operation on high performance parallel computing platforms such as the SGI/Cray Origin2000 (O2K). For spectral simulations without interfrequency exchange, the solution of Eq. (1) for each monochromatic component leads to an independent system of linear equations. These equations are solved using distributed clusters of shared-memory multiprocessors (SMPs) which have to communicate and share the workload, e.g., via a Message Passing Interface, MPI. Individual wave components are distributed to multiple processors via MPI and load-balanced through the Manager-Worker model (Foster, 1997; Bova *et al.*, 2000). At the second level, matrix operations are parallelized since most of the CPU-time for each wave component is utilized in the solution of the linear system

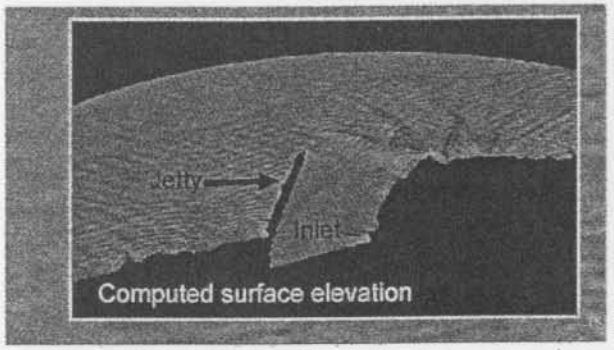

Fig. 6. Simulation of spectral wave conditions in Ponce de Leon Inlet, after Bova *et al.* (2000); instantaneous snapshot of sea surface.

of equations. For conjugate gradient solvers, 90% of the CPU time is spent on matrix-vector products and inner product kernels. Therefore, OpenMP (OARB 1997) may be used to parallelize the kernels. Two-level parallelization schemes can use OpenMP to accelerate the solution for each component and MPI to simultaneously obtain solutions to multiple incident wave components. More details regarding parallelization schemes for harbor wave models may be found in Bova *et al.* (2000) who report a reduction in run times by a factor of 250–580 compared with serial codes for an application in Ponce de Leon Inlet (Florida). A problem with nearly 300 input spectral components was solved on a 25 square km domain containing 235,000 nodes in 72 hours. An example from Bova *et al.* (2000), shown in Fig. 6, suggests that the simulation produces, qualitatively, a sea-surface that looks realistic. Model results for this site are discussed in greater detail by Zhao *et al.* (2000).

4. Incorporation of Additional Mechanisms

As noted earlier, Eq. (1) incorporates the effects of refraction, diffraction and reflection induced by any nonhomogeneity in the model domain. Equation (5) is an extension of Eq. (1) that includes, in addition, the effects of friction and wave breaking. Similar extensions are possible to include the effects of wave-current interaction, wave-wave interaction and of steep slopes. The modeling of these mechanisms in the context of the elliptic equation, Eq. (1), is described in this section.

4.1. *Dissipation*

In Eq. (5), W represents the combined effects of friction and breaking which may be separated as follows,

$$W = w/C_g + \gamma, \tag{30}$$

where w is the friction coefficient defined by Dalrymple *et al.* (1984) and γ is a breaking factor. These coefficients are empirical and parametrizations for these have been described by Dalrymple *et al.* (1984), Tsay *et al.* (1989) and Chen (1986) for friction, and by Battjes and Janssen (1978), Dally *et al.* (1985), Massel (1992), Chawla *et al.* (1998) and Isobe (1999) for breaking. Some of these parameterizations have been extensively validated against field data (e.g., Larson, 1995; Kamphuis, 1994). We do not repeat the parameterizations here; rather, we note that they are all dependent on the wave amplitude.

Published studies demonstrating the effects of friction in harbor models (e.g., Chen, 1986; Tsay *et al.*, 1989; Demirbilek and Panchang, 1998; Kostense *et al.*, 1986) have estimated w on the basis of the incident wave amplitude. It is then easy to pre-specify w while solving Eq. (5). These studies appear to show that friction can change the magnitude of resonant peaks in harbor models quite substantially; at other frequencies, the effect seems to be minimal. Jeong *et al.* (1996) and Moffatt & Nichol Engineers (1999) have attempted to utilize W to include harbor entrance losses, however, no details regarding the modeling technique are presented.

In general, however, since both w and γ are functions of the wave amplitude which is unknown *a priori* inside the domain, their inclusion makes the problem nonlinear and requires iteration. For the first iteration, W is set equal to 0 and Eq. (1) is solved (e.g., nonbreaking solutions are obtained). The resulting wave heights are used to estimate W via the parameterizations for w and γ and Eq. (5) is solved. The process is repeated until convergence is obtained.

Since dissipation (especially breaking) occurs outside the computational domain also, open boundary conditions like Eqs. (13), (15) and (16) may not be appropriate. Inclusion of breaking inside the domain and its exclusion in the exterior descriptions create artificial discontinuities along the open boundary, especially in shallow areas, and consequently, spurious effects would propagate into the model domain. In this event, Eq. (20) is a more appropriate description of the exterior and may be used to develop the necessary boundary conditions. A digitized bathymetry file is used to obtain the depths $d(x)$ along transect 1. These depths are interpolated onto uniformly spaced nodes and the wave properties C, C_g and k are calculated. Equation (20) may be easily solved by finite-differences using boundary conditions, Eqs. (24) and (25). Again, iterations are required because W is not known initially. When the solutions converge, the procedure is repeated for transect 2. These converged solutions of Eq. (20) along transects 1 and 2 include, albeit in a one-dimensional sense, the effects of dissipation and hence constitute more appropriate forcing functions than Eqs. (13), (15) and (16) do. ϕ_0 along the semicircular open boundary is obtained via Eq. (26).

Performing nonlinear iterations within the model domain as W varies from iteration to iteration can be time-intensive. We have explored the possibility of combining the iterative conjugate gradient methods for the linear system with the iterations required for the nonlinear modeling, i.e., the conjugate gradient iterates obtained while solving Eq. (28) were perturbed by upgrading W

periodically. Unfortunately, this maneuvering destroys the robust convergence properties of the conjugate gradient solvers for Eq. (28). At present, each linear system, for a specified W, must be completely solved until convergence is obtained and the whole procedure repeated with a new W. More effective methods to accelerate the solution need to be developed.

Zhao *et al.* (2000) developed a finite-element model using Eqs. (6), (20) and (27) to formulate the boundary conditions and applied it to several tests involving breaking. These tests involved a sloping beach, a bar-trough bottom configuration, shore-connected and shore-parallel breakwaters on a sloping beach, and two field cases in the North Sea and Ponce de Leon Inlet (Florida). Five breaking formulations, given by Battjes and Janssen (1978), Dally *et al.* (1985), Massel (1992), Chawla *et al.* (1998) and Isobe (1999), were examined. They found that the Isobe (1999) criterion was difficult to use within the context of the elliptic model and that the absence of a lower breaking limit generally contributed to excessive dissipation (compared with data) in the Chawla *et al.* (1998) and Massel (1992) formulations. In general, the formulations of Battjes and Janssen (1978) and Dally *et al.* (1985) were found to be the most robust from the point of view of incorporation into an elliptic model based on Eq. (5) and to provide excellent results compared to data.

For simulations involving several spectral components, Zhao *et al.* (2000) examined two approaches. In the first approach, complete simulations were made one at a time for all monochromatic components where the amplitude of each component was used in the relevant breaking formula. The results were subsequently assembled using linear superposition. They found that this approach led to some overestimation compared with data; this was attributed to the individual component amplitudes being too small to induce breaking in the model. In view of this overestimation, a second approach was considered where the breaking factor was calculated on the basis of the significant wave height instead of the component wave height. This approach eliminates the independence of individual component simulations, thereby changing the overall model numerics. With the second approach, one round of nonlinear iterations for all components must be performed, the significant wave height is calculated at each grid point and this larger wave height is used to estimate the breaking factor (Chawla *et al.*, 1998). This approach led to the initiation of breaking occurring further offshore in the case of their simulations of wave transformation around Ponce de Leon Inlet. An example of the model simulations near the US Army Field Research Facility at Duck, North Carolina, is shown in Fig. 7 for an input wave condition given by a significant wave height of 2.3 meters.

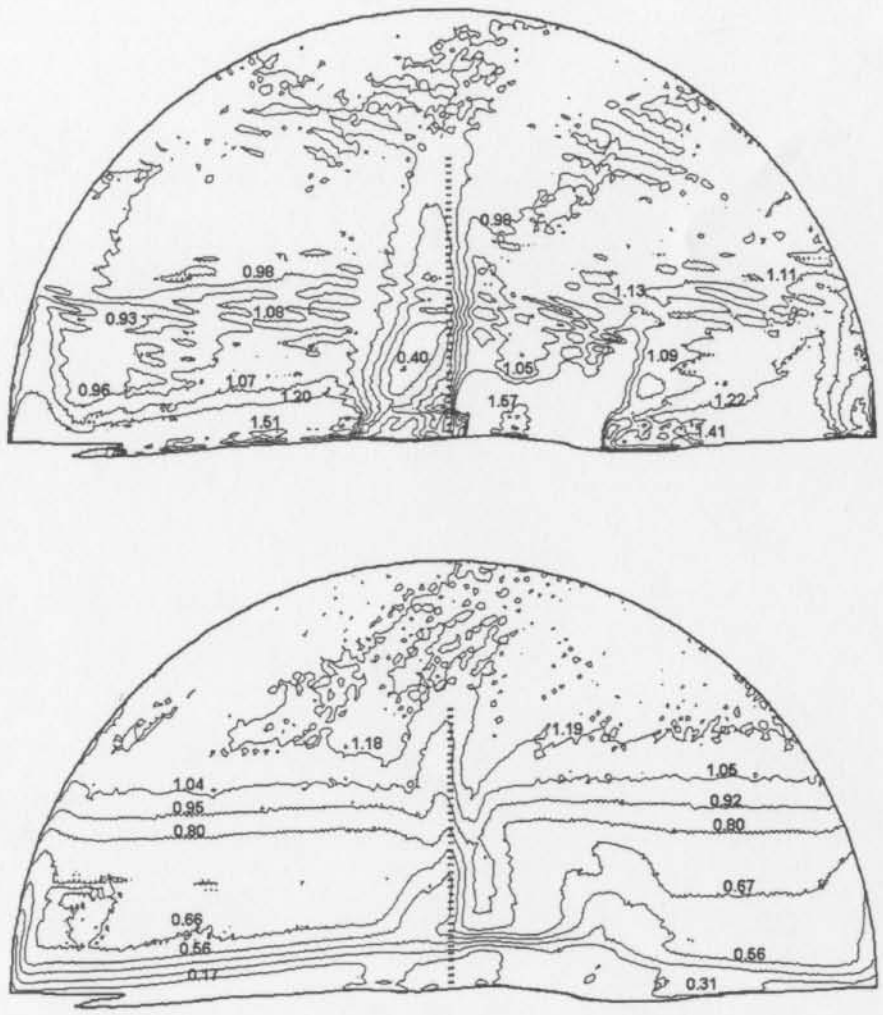

Fig. 7. Modeled wave amplitudes (m) at FRF Duck. Top, no breaking; Bottom, breaking based on significant wave height.

A complex pattern of waves is created in the middle of the domain due to the complicated bathymetry. Clearly, breaking plays an important role (the dots aligned in the shore-perpendicular direction in the middle of these figures represent circular piles which were assigned full reflection). These simulations were performed with 208 spectral components for a storm in 1996. The

simulations took 265 hours CPU time using 41 processors and ran nonstop for about 3 days on the US Army Corps of Engineers super-computer. Comparison to field data and other details are provided elsewhere.

4.2. *Wave-current interaction*

Many coastal regions experience high background currents. Wave propagation is influenced by these currents (e.g., waves opposing the currents become larger and vice-versa). Based on the derivation by Kirby (1984), one may incorporate currents in Eq. (5) as follows,

$$\nabla \cdot (CC_g \nabla\phi) - \nabla \cdot (\mathbf{U}(\mathbf{U} \cdot \nabla\phi)) + \left(\frac{C_g}{C}\sigma_r^2 + iC_g\sigma_r W + \sigma^2 - \sigma_r^2 + i\sigma\nabla \cdot \mathbf{U} \right)$$

$$\phi + 2i\sigma\mathbf{U} \cdot \nabla\phi = 0\,, \tag{31}$$

where $\mathbf{U}(x,y)$ = current vector (provided by a flow model), $\sigma_r = \sigma - \mathbf{k} \cdot \mathbf{U}$ = relative frequency. ($\sigma_r^2 = gk \tanh(kd)$; $C = \sigma_r/k$). Several sophisticated hydrodynamic models are available nowadays for obtaining the desired flowfield information $\mathbf{U}(x,y)$. When hydrodynamic models provide three-dimensional flowfields, the vertical dependence may be removed for use in Eq. (31) via the "equivalent uniform current" defined by Hedges and Lee (1992); this quantity is obtained by vertically averaging the current over a depth εL over the water column where $\varepsilon L = (1/k)\tanh(kd)$.

The generalized mild-slope wave equation, Eq. (31), is still elliptic and may be solved by the techniques noted previously. For a prespecified $\mathbf{U}(x,y)$, a linear system of equations like Eq. (28) results. However, to compute the Doppler shift in the wave frequency ($\sigma_r = \sigma - \mathbf{k} \cdot \mathbf{U}$), the wave vector $\mathbf{k}$ is needed. While the *magnitude* of $\mathbf{k}$ is known *a priori* from the dispersion relation, Eq. (2), its *direction* is not. This problem may be resolved by first solving Eq. (31) without the effects of wave-current interaction, obtaining an estimate of the local wave direction, computing the relative frequency $\sigma_r = \sigma - \mathbf{k} \cdot \mathbf{U}$, solving Eq. (31) again, revising the wave direction, and repeating until the model runs converge. Such an approach has been taken by Kostense *et al.* (1988); Li and Anastasiou (1992), however, prefer not to calculate the direction of k in view of the computational burden. While their results for one test-case (pertaining to waves approaching a rip current on a sloping beach) are reasonable, iterations are indeed necessary for complex flowfields.

Further difficulties arise in the specification of open boundary conditions. Published studies using the elliptic model of Eq. (31) have assumed that currents are absent on this boundary. Research is needed to develop open boundary conditions that include the effects of currents (an extension of Eq. (20) is possible for the case of currents varying only in the cross-shore direction outside the computational domain).

4.3. *Wave-wave interaction*

By including most of the nonlinear terms in the vertical integration of the three-dimensional Laplace equation, Kaihatu and Kirby (1995) obtained an extension of Eq. (1) that incorporates wave-wave interactions. Expressing the potential in terms of harmonics as:

$$\phi(x,y,z,t) = \sum_{n=1}^{N} f_n(k_n,d,z)\phi_n(k_n,\omega_n,x,y,t)\,, \tag{32}$$

where,

$$f_n = \frac{\cosh k_n(d+z)}{\cosh k_n d}\,, \tag{33}$$

and performing an integration over the vertical modifies Eq. (5) as follows,

$$\nabla_h \cdot \lfloor (CC_g)_n \nabla\phi_n \rfloor + k_n^2 (CC_g)_n \phi_n + i(C_g\sigma W)_n\phi_n$$

$$= -\frac{i}{4}\left[\sum_{l=1}^{n-1} 2\sigma_n \nabla\phi_l \cdot \nabla\phi_{n-l} + \sigma_l\phi_l\nabla^2\phi_{n-l} + \sigma_{n-l}\phi_{n-l}\nabla^2\phi_l \right.$$

$$\left. + \frac{\sigma_l\sigma_{n-l}\sigma_n}{g^2}(\sigma_l^2 + \sigma_l\sigma_{n-l} + \sigma_{n-l}^2)\phi_l\phi_{n-l} \right]$$

$$-\frac{i}{2}\left[\sum_{l=1}^{N-n} 2\sigma_n \nabla\phi_l^* \cdot \nabla\phi_{n+l} + \sigma_{n+l}\phi_{n+l}\nabla^2\phi_l^* - \sigma_1\phi_l^*\nabla^2\phi_{n+l} \right.$$

$$\left. - \frac{\sigma_l\sigma_{n+1}\sigma_n}{g^2}(\sigma_l^2 - \sigma_l\sigma_{n+1} + \sigma_{n+1}^2)\phi_l^*\phi_{n+1} \right]\,, \tag{34}$$

in which ϕ_l^* = complex conjugate value of ϕ_l.

Similar equations were also derived by Tang and Ouellet (1997) who have further demonstrated that this type of extension provides the governing equation, Eq. (1), with the same level of nonlinearity as that in Boussinesq wave models. This is particularly noteworthy since models based on Eq. (1) or

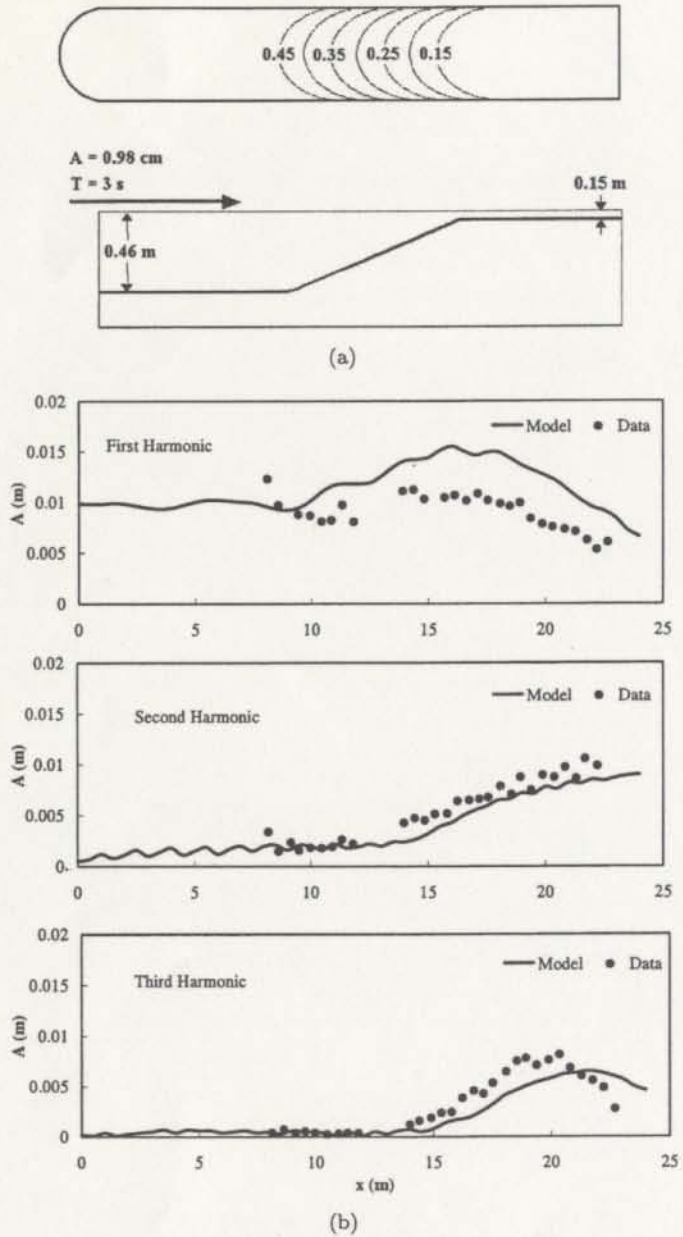

Fig. 8. (a) Bathymetry (m) of Whalin (1971) used for wave-wave interaction study, (b) wave height comparison for wave-wave interaction.

Eq. (5) simultaneously offer the computational stability and the advantages of finite-element gridding in harbors and complex coastal areas (which Boussinesq models sometimes lack). From the perspective of the solution technique, the coupling of harmonics represented by the right hand-side of Eq. (34), if prespecified, leads to a linear system of equations like Eq. (28). However, for a given component ϕ_n, the other components constituting the right hand side are not known *a priori*. Again, an iterative technique must be used where the values from the previous round can be used to calculate the right hand side. Figure 8 shows a finite element model simulation (based on Eq. (34)) of wave propagation and interaction over the "tilted cylinder" bathymetry of Whalin (1971). The results match the laboratory data of Whalin (1971) very well and shows that higher harmonics can build up from zero to a magnitude similar to the linear solution and can hence contribute much to the overall solution (hitherto the coupling represented by the right hand side was included only in simple (parabolic approximation) models; e.g., Tang and Ouellet, 1997 and Kaihatu and Kirby, 1995).

4.4. *Combined nonlinear mechanisms*

Equation (34) contains the effects of two of the additional mechanisms described so far, i.e., wave-wave interactions and dissipation. By rederiving Eq. (34) on a moving frame of reference, the equation may be extended to simultaneously include the effects of wave-current interaction also (Kaihatu and Kirby, 1995). As demonstrated above, the modeling procedures for each of these mechanisms are individually nonlinear and require numerical iterations. However, combining all the nonlinear effects in numerical simulations has as yet been unexplored. An efficient model must juxtapose iterations and also assure convergence. Further, appropriate tests for the enhanced model are not readily available (especially for the combination of wave-wave and wave-current interactions). For systematic model verification, data isolating and combining these mechanisms are needed. In that regard, the numerical advancements appear to be preceding data availability.

4.5. *Steep-slope effects*

Unlike the inclusion of the nonlinear mechanisms described above, overcoming the "mild slope" requirement discussed in Sec. 1 is relatively easy. Massel (1993), Porter and Staziker (1995), Chamberlain and Porter (1995), and

Chandrasekera and Cheung (1997) developed extensions of Eq. (1) to include steep-slope effects. Their extensions may be described by the following equation,

$$\nabla \cdot (CC_g \nabla \phi) + (k^2 CC_g + d_1(\nabla h)^2 + d_2 \nabla^2 h)\phi = 0\,, \tag{35}$$

where d_1 and d_2 are functions of local depths. Reference may be made to these publications for the various definitions of d_1 and d_2; in general, though, differences in the proposed definitions of these functions impact model results to a very small extent. The steep-slope terms are fairly straightforward to include in the model because they are linear. Further, they have the advantage of being "automatic", i.e., they have little contribution for mild slopes, do not change the solution technique and the additional computational demand is negligible. However, steep slopes lead to breaking and model performance in the vicinity of steep slopes will involve iterations (an analytical model has been developed by Massel and Gourlay (2000) to include breaking and steep-slope effects near coral reefs).

5. Application to Harbors

So far, we have described various developments made in recent years to construct more reliable models based on Eq. (1) for use in domains with arbitrary shape and bathymetry. In this section, we describe application of one such model to the practical problem of simulating harbor resonance in the Los Angeles/Long Beach Harbor complex (Fig. 1) and in Barber's Point Harbor (Hawaii). Both harbors are undergoing considerable renovation to accommodate increased shipping. A finite-element model called CGWAVE was developed to solve Eq. (5) using Eqs. (6), (18), (20) and (27) to formulate the boundary conditions. The Surface Water Modeling System (Zundell *et al.*, 1998) was used for grid generation.

5.1. *Simulations in the Los Angeles/Long Beach Harbor complex*

The Los Angeles/Long Beach Harbor complex (Fig. 1) is one of the largest harbors in the world; therefore, the model domain is quite large covering an area of approximately 120 square km. Bathymetric input was obtained by digitizing NOAA chart number 18749. For numerical modeling, a grid containing 285,205 triangular finite elements was developed. It was based on a resolution

of 10 points per wavelength for a 30-second wave. The two one-dimensional transects in the exterior were extended in the offshore direction to a distance of 9.2 km beyond which the depth was assumed to be constant. At this location, the input wave was specified.

For initial quality control simulations, the coastal reflectivity was initially set equal to zero (i.e., fully absorbing) since this case is easier to examine qualitatively than the case when a large number of reflections are present. Figure 9 shows the phase diagram for a 50 second wave. The results appear to be quite satisfactory. A reduction in the wavelength in the onshore direction is evident. No spurious boundary effects are seen. Penetration through the breakwater gaps is precisely as one would expect. Bending of the crests as they approach from onshore also indicates a correct reproduction of refractive effects.

For further simulations, the coastal boundary was assumed to be fully reflecting (both inside the model and for the one-dimensional transects). Also, the geometry of the offshore breakwaters was changed. These breakwaters are known to be permeable to waves (e.g., Chiang, 1987) and it is hence not appropriate to consider them as closed boundaries. Permeable structures cannot be easily handled within the context of an elliptic boundary value problem.

Fig. 9. Modeled phase diagram for Los Angeles/Long Beach Harbor complex; 50 second obliquely incident wave.

One approach may be to treat the breakwater as a water area and ascribe an appropriate dissipation factor in that region. We used an alternative approach whereby the breakwater was divided into several segments so that energy could propagate through gaps in the breakwater. 50% of the breakwater length was opened up by means of numerous gaps interspersed among several solid segments.

Seabergh and Thomas (1995) conducted hydraulic model simulations for this complex at the US Army Waterway Experiment Station in Vicksburg, Mississippi. They collected data at several gages, shown in Fig. 1, for various harbor plans. The bathymetric data used for numerical modeling obtained from the more recent NOAA chart was a reasonable approximation of the harbor geometry described as "Stage II" by Seabergh and Thomas (1995). However, neither the bathymetry data nor the boundary geometries used in the two studies were identical.

Seabergh and Thomas (1995) performed their hydraulic model experiments for a large number of input frequency components varying from 30 seconds to 512 seconds. At each gage location, the amplification factor was measured for several frequencies and a resonance curve was developed. These curves were found to be extremely noisy, i.e., the response varied quite rapidly with frequency at the gages (see example in Fig. 10). For convenience of analysis, therefore, they partitioned the data into three groups: short period waves (30 s

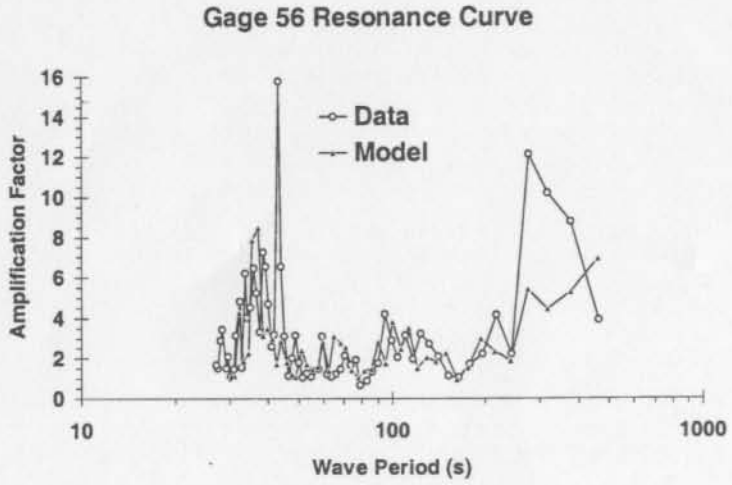

Fig. 10. Resonance curve at Gage 56.

to 42 s), medium period waves (42 s to 205 s) and long period waves (205 s to 512 s). For each gage, the amplification factors within each group were averaged over the respective frequencies.

Numerical simulations were performed for three incident angles, for normal incidence and for 30° on either side of it, to account for the effects of the wave maker. The results of the three directional inputs were averaged for each frequency. The exact location of each gage was not known, so results in the general vicinity of the gage as determined from Fig. 1 were extracted and averaged over the frequency bands stated earlier. In all, simulations were made for 10, 30 and 17 frequency components in the three bands. These components are irregularly spaced and correspond approximately to the discrete frequency components used by Seabergh and Thomas (1995) in their hydraulic model simulations.

An example of the modeled resonance curve is shown in Fig. 10. At $T = 45$ s, the lab data show a remarkably high amplification that the model underpredicts; conversely, for T between 300 s and 400 s, the model value is greater than the hydraulic model data. The overall results for all gages, using the averaging described above, are compared against the hydraulic model data in Fig. 11. In general, the numerical simulation predicts the response at the gages as well as the hydraulic model data. The agreement is quite good for the short and medium period waves. Greater discrepancy is seen for the long waves which also exhibit greater gage-to-gage variability. For the long waves, there seems to be systematic overprediction near certain gages. These discrepancies could be attributed to several factors. First, the two bathymetry sets are not identical and the high variability implies that small differences in the geometry can result in large differences in the response. The location of the input wave is also different in the hydraulic and numerical models. Further, the exterior sea is bounded in the hydraulic model, thus, possibly preventing radiation out to the open sea. Finally, reflection coefficients and the degree of permeability of the breakwaters are not sufficiently well-known.

It is of course possible to introduce dissipation and/or adjust reflection coefficients or breakwater closure to tune the model better so that a calibrated model for the Los Angeles/Long Beach complex would be available for future use. However, there is no assurance that the hydraulic model is the true benchmark. The high level of agreement between the hydraulic model and numerical model results for the short and medium period waves and the moderate agreement for the long period waves indicates that the performance of the numerical and hydraulic models are certainly compatible, although not identical.

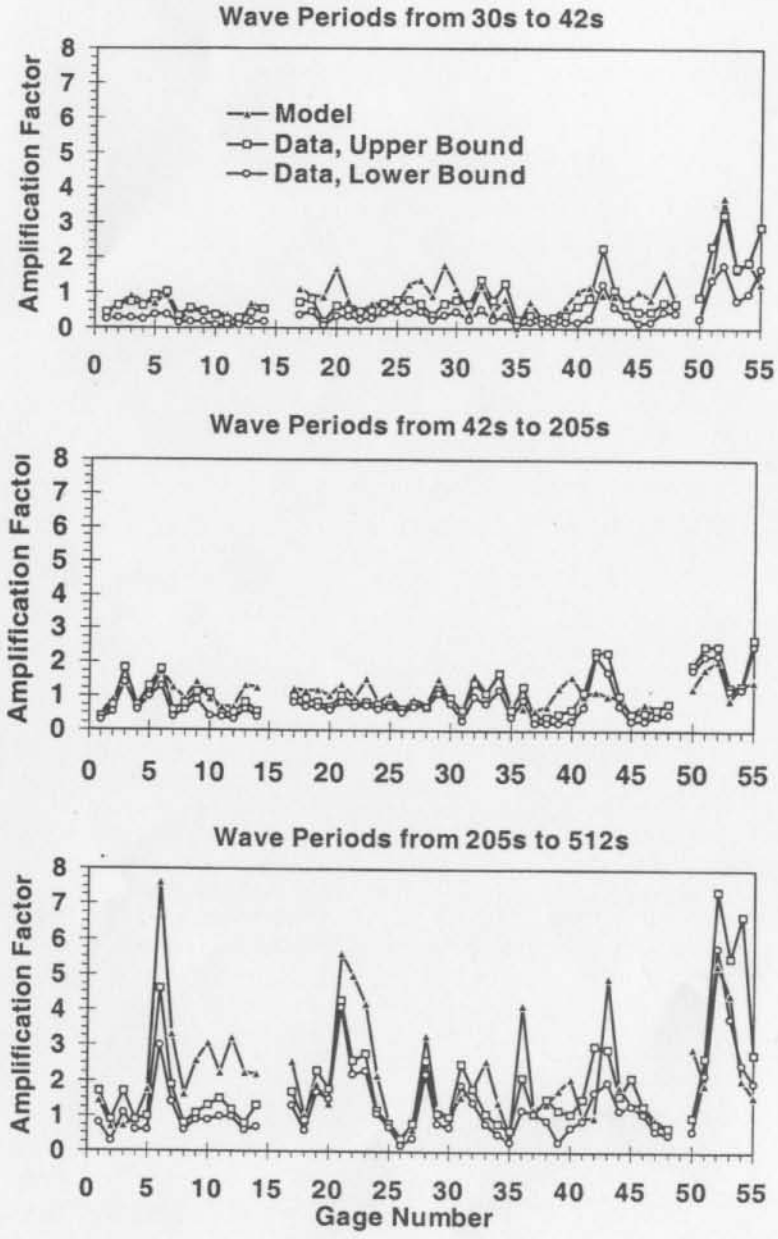

Fig. 11. Wave height comparison for Los Angeles/Long Beach Harbor complex.

5.2. *Simulations in Barber's Point Harbor*

Seiches in Barber's Point Harbor (Hawaii) have been studied by Okihiro *et al.* (1993) and Okihiro and Guza (1996). Okihiro *et al.* (1993) also used a numerical model (Chen and Houston, 1987) based on Eq. (5) with Eqs. (15)–(17) describing the open boundary conditions. Such a model, as noted earlier, confronts the modeler with having to select a constant exterior depth and to assume that the exterior coastline is fully reflecting. Further, this model solves Eq. (28) by Gausian elimination. As noted earlier, this creates storage problems and hence allows only coarse resolution for some frequencies. To overcome these limitations, Eqs. (18), (20) and (27) were used to formulate the open boundary conditions.

Bathymetric data used by Okihiro *et al.* (1993) were used to develop a new grid containing about 65,065 elements. The model was run for 136 frequency components. Full reflection was used on all closed boundaries. Field data were available at four locations inside the harbor (denoted by East, West, North and South gages); see Fig. 12. Data were also available at a gage outside the harbor (denoted by "offshore" gage in Fig. 12); these were used to normalize the amplification factors inside the harbor. Model results are

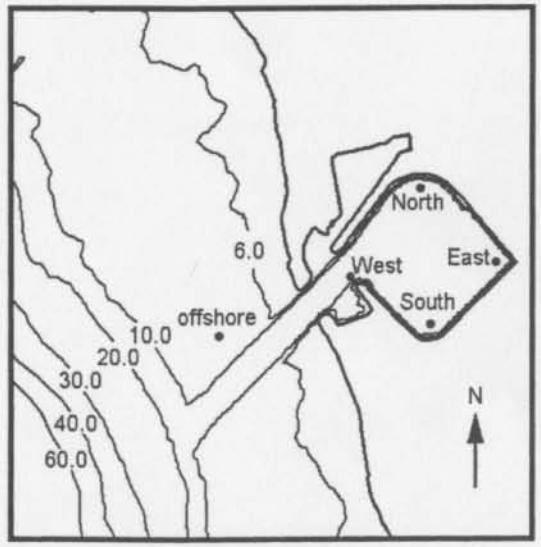

Fig. 12. Barber's Point Harbor, bathymetry and gage locations.

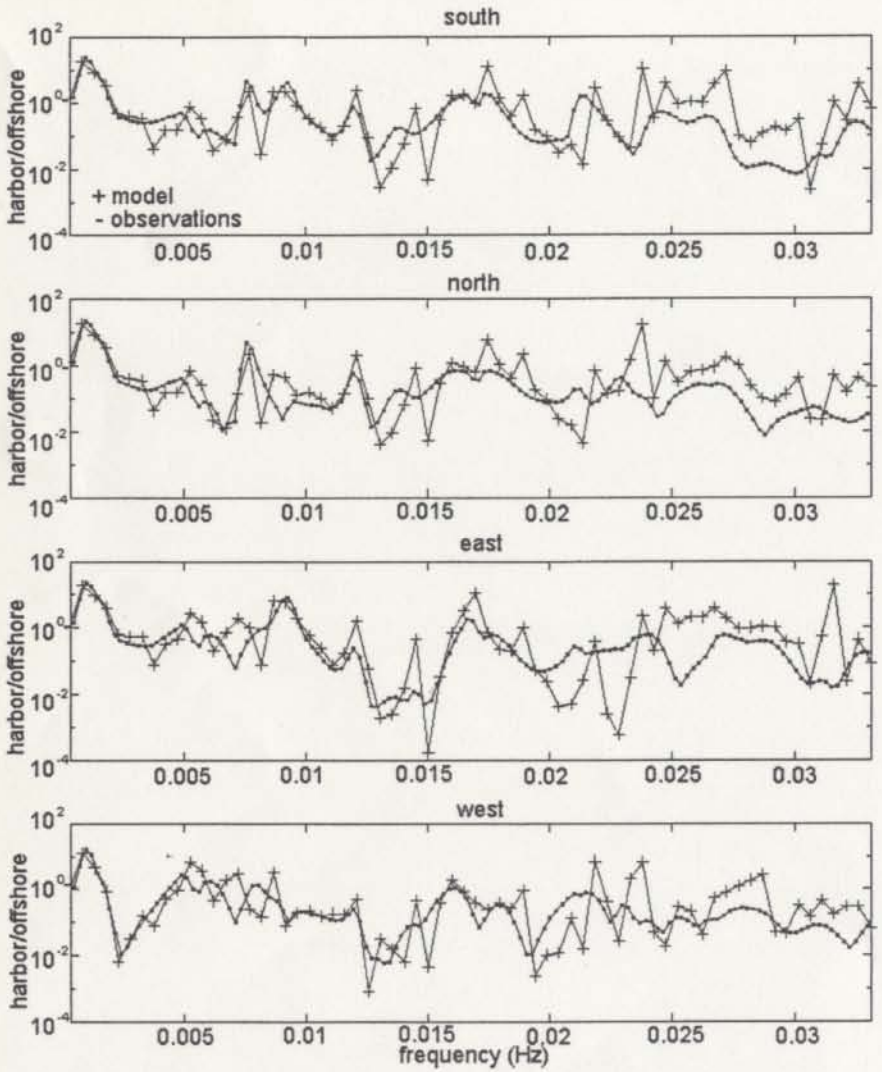

Fig. 13. Wave height comparison for Barbers Point Harbor.

compared against field data in Fig. 13. There is fairly good agreement between the model calculations and the measurements especially for the long periods. For the short periods, there appears to be some overprediction by the model. This is attributed to the fact that shorter waves experience less reflection. The

simulations with a lower reflection coefficient for these waves and more detailed results will be presented elsewhere. However, the results at all four locations inside the harbor are a fairly reasonable reproduction of the field data.

6. Concluding Remarks

In this paper, we have provided a review of recent developments in simulating ocean waves with models based on the elliptic refraction-diffraction equation. In general, finite element models appear to be best suited for practical applications covering the full spectrum of waves to which a harbor may be exposed. (Some practical applications may be found, for example, in Tang *et al.*, 1999; Pos *et al.*, 1989; Mattioli, 1996; Kostense *et al.*, 1988). Advances in the treatment of boundary conditions and of matrix systems associated with the discretized equations have made it possible to eliminate many of the difficulties that led to inferior solutions. They have also eliminated the need for approximations of the elliptic model. Further, the advances reduce the burden on the modeler who does not have to test the sensitivity of model results to unrealistic assumptions (such as constant depths in the exterior). Applications to the Los Angeles/Long Beach Harbor region and to Barber's Point Harbor presented here demonstrate that finite element modeling with the techniques described in this paper produces results that are at least as reliable as those obtained by other methods. Inclusion of additional mechanisms like dissipation, wave-wave interactions, wave-current interactions and steep slope effects can enhance the usefulness of these models. However, how a model will behave when these effects are combined is not yet clear. Further research in modeling methods as well as data where some of these effects can be combined and isolated are desirable.

Acknowledgments

Partial support for this work was provided by the Office of Naval Research, the Maine Sea Grant Program and the National Sea Grant Office. Many of the developments described here were made with the assistance of five graduate students at the University of Maine (Karl Schlenker, Wei Chen, Luizhi Zhao, Doncheng Li and Khalid Zubier) and Dr. Michele Okihiro of the Scripps Institution of Oceanography. Their contributions are gratefully acknowledged. Permission to publish this paper was granted by the Chief, Corps of Engineers, to publish this paper.

References

Battjes, J. A. and J. Janssen (1978). Energy loss and set-up due to breaking of random waves. *Proc. 16th Int. Conf. Coastal Eng.*, ASCE, New York, 569–587.

Berkhoff, J. C. W. (1976). *Mathematical Models for Simple Harmonic Linear Water Waves. Wave Refraction and Diffraction*, Publ. 163, Delft Hydraulics Laboratory.

Beltrami, G. M., G. Bellotti, P. De Girolamo, and P. Sammarco (2000). Treatment of wave breaking and total absorption in a mild-slope equation FEM model. *J. Waterway, Port, Coastal & Ocean Eng.* To appear.

Booij, N. (1981). *Gravity Waves on Water with Nonuniform Depth and Current*, Ph.D. Thesis, Technical Univ. of Delft, The Netherlands.

Bova, S. W., C. P. Breshears, C. Cuicchi, Z. Demirbilek, and H. A. Gabb (2000). Dual-level parallel analysis of harbor wave response using MPI and OpenMPI. *Int. J. High Performance Comput. Appl.* **14**(1): 49–64.

Chamberlain, P. G. and D. Porter (1995). The modified mild-slope equation. *J. Fluid Mech.* **291**: 393–407.

Chandrasekera, C. N. and K. F. Cheung (1997). Extended linear refraction-diffraction model. *J. Waterway, Port, Coastal & Ocean Eng.* **123**(5): 280–286.

Chawla, A., H. T. Ozkan-Haller, and J. T. Kirby (1998). Spectral model for wave transformation and breaking over irregular bathymetry. *J. Waterway, Port, Coastal & Ocean Eng.* **124**: 189–198.

Chen, H. S. (1986). Effects of bottom friction and boundary absorption on water wave scattering. *Appl. Ocean Res.* **82**(2): 99–104.

Chen, H. S. (1990). Infinite elements for water wave radiation and scattering. *Int. J. Numer. Meth. Fluids* **11**: 55–569.

Chen, H. S. and J. R. Houston (1987). Calculation of water level oscillations in harbors. Instructional Rept. CERC-87-2, Waterways Expt. Stn., Vicksburg, Mississippi.

Chiang, W.-L. (1988). Modeling long and intermediate waves in a harbor. *Appl. Math. Modeling* **12**: 423–428.

Dally, W. R., R. G. Dean, and R. A. Dalrymple (1985). Wave height variation across beaches of arbitrary profile. *J. Geophys. Res.* **90**(c6): 11917–11927.

Dalrymple, R. A., J. T. Kirby, and P. A. Hwang (1984). Wave diffraction due to areas of high energy dissipation. *J. Waterway, Port, Coastal & Ocean Eng.* **110**(1): 67–79.

Demirbilek, Z., B. Xu, and V. G. Panchang (1996). Uncertainties in the validation of harbor wave models. *Proc. 25th Int. Coastal Eng. Conf.*, 1256–1267.

Demirbilek, Z. and V. G. Panchang (1998). CGWAVE: A coastal surface water wave model of the mild slope equation, Tech. Rept. CHL-98-26, US Army Corps. of Engineers Waterways Expt. Stn., Vicksburg, MS 39180.

Dickson, W. S., T. H. C. Herbers, and E. B. Thornton (1995). Wave reflection from breakwater. *J. Waterway, Port, Coastal & Ocean Eng.* **121**(5): 262–268.

Dingemaans, M. W. (1997). *Water Wave Propagation over Uneven Bottoms*. World Scientific. Singapore.

Ebersole, B. A. (1985). Refraction-diffraction model for linear water wave. *J. Waterway, Port, Coastal & Ocean Eng.* **111**(6): 939–953.

Foster, I. (1997). *Designing and Building Parallel Programs*, Addison-Wesley Publ. Co., Reading, MA.

Givoli, D. (1991). Nonreflecting Boundary Conditions. *J. Comput. Phys.* **94**: 1–29.

Hedges, T. S. and B. W. Lee (1992). The equivalent uniform current in wave-current interaction computations. *Coastal Eng.* **16**: 301–311.

Hurdle, D. P., J. K. Kostense, and P. Bosch (1989). Mild slope model for the wave behavior in and around harbors and coastal structures. In: *Advance in Water Modeling and Measurement*, ed. M. H. Palmer. BHRA, The Fluid Eng. Centre, Cranfield, England. 307–324.

Irons, P. (1970). A frontal solution program for finite element analysis. *Int. J. Numer. Meth. Eng.* **2**: 5–32.

Isaacson, M. and S. Qu (1990). Waves in a harbor with partially reflecting boundaries. *Coastal Eng.* **14**: 193–214.

Isaacson, M., E. O'Sullivan, and J. Baldwin (1993). Reflection effects on wave field within a harbor. *Can. J. Civ. Eng.* **20**(3): 386–397.

Isobe, M. (1999). Equation for numerical modeling of wave transformation in shallow water. In: *Developments in Offshore Engineering*, Chapter 3, ed. J. B. Herbich. Gulf Publishing, Houston. 101–162.

Jeong, W. M., J. W. Chae, W. S. Park, and K. T. Jung (1996). Field measurements and numerical modeling of harbor oscillations during storm waves. *Proc. 25th Int. Conf. Coastal Eng.* ASCE, New York. 1268–1279.

Jones, N. L. and D. R. Richards (1992). Mesh generation for estuarine flow models. *J. Waterway, Port, Coastal & Ocean Eng.* **118**(6).

Kamphuis, J. W. (1994). Wave height from deep water through breaking zone. *J. Waterway, Port, Coastal & Ocean Eng.* **120**(4): 347–367.

Kaihatu, J. and J. T. Kirby (1995). Nonlinear transformation of waves in finite water depth. *Phys. Fluids* **7**(8): 1903–1914.

Kirby, J. T. (1984). A note on linear surface wave-current interaction over slowly varying topography waves. *J. Geophys. Res.* **89**(c1): 745–747.

Kirby, J. T. (1986). Higher order approximation in the parabolic equation method for water waves. *J. Geophys. Res.* **91**(c1): 933–952.

Kostense, J. K., K. L. Meijer, M. W. Dingemans, A. E. Mynett, and P. van den Bosch (1986). Wave energy dissipation in arbitrarily shaped harbors of variable depth. *Proc. 20th Int. Conf. Coastal Eng.* 2002–2016.

Kostense, J. K., M. W. Dingemans, and P. van den Bosch (1988). Wave-current interaction in harbors. *Proc. 21th Int. Conf. Coastal Eng.* **1**: 32–46. ASCE, New York.

Lee, J. J. and F. Raichlen (1972). Oscillations in harbors with connected basins. *J. Waterways, Harbors, and Coastal Eng. Div.* **98**: 311–332. ASCE.

Lennon, G. P., P. L.-F. Liu, and J. A. Liggett (1982). Boundary integral solutions of water wave problems. *J. Hydr. Div. ASCE* **108**: 921–931.

Li, B. (1994a). A generalized conjugate gradient model for the mild slope equation. *Coastal Eng.* **23**: 215–225.

Li, B. (1994b). An evolution equation for water waves. *Coastal Eng.* **23**: 227–242.

Li, B. and K. Anastasiou (1992). Efficient elliptic solvers for the mild-slope equation using the multigrid method. *Coastal Eng.* **16**: 245–266.

Li, B., D. E. Reeve, and C. A. Fleming (1993). Numerical solution of the elliptic mild-slope equation for irregular wave propagation. *Coastal Eng.* **20**: 85–100.

Larson, M. (1995). Model for decay of random waves in surf zone. *J. Waterway, Port, Coastal & Ocean Eng.* **121**(1): 1–12.

Massel, S. R. (1992). Inclusion of wave-breaking mechanism in a modified mild-slope model. In: *Breaking Waves IUTAM Symposium*, Sydney/Australia, 1991. eds. M. L. Banner and R. H. J. Grimshaw. Springer-Verlag, Berlin Heidelberg, 1992. 319–324.

Massel, S. R. (1993). Extended refraction-diffraction equation for surface waves. *Coastal Eng.* **19**: 97–126.

Massel, S. R. and M. R. Gourlay (2000). On the modeling of wave breaking and set-up on coral reefs. *Coastal Eng.* **391**: 1–27.

Marchuk, G. I. (1975). *Methods of Numerical Mathematics. Applications of Mathematics.* Springer-Verlag, New York.

Mattioli, F. (1996). Dynamic response of the Lido channel to wave motion in the presence of movable barriers. *Il Nuovo Cimento* **19c**(1): 177–194.

Mei, C. C. (1983). *The Applied Dynamics of Ocean Surface Waves.* John Wiley, New York.

Moffatt & Nichol Engineers (1999). San Pedro Bay Harbor Resonance Model for LA/LB Complex. User's Manual. 250 W. Wardlow Road, Long Beach, CA 90807.

OARB (1997). OpenMP Fortran Application Program Interface. *OpenMP Architecture Review Board (OARB)* v1.0, http://www.openmp.org, October 1997.

Okihiro, M. and R. T. Guza (1996). Observations of Seiche forcing and amplification in three small harbors. *J. Waterway, Port, Coastal & Ocean Eng.* **122**(5): 232–238.

Okihiro, M., R. T. Guza, and R. J. Seymour (1993). Excitation of Seiche observed in a small harbor. *J. Geophys. Res.* **122**(5): 232–238.

Oliveira, F. S. B. F. and K. Anastasiou (1998). An efficient computational model for water wave propagation in coastal regions. *Appl. Ocean Res.* **20**: 263–271.

Panchang, V. G., B. Cushman-Roisin, and B. R. Pearce (1988). Combined refraction-diffraction of short waves for large coastal regions. *Coastal Eng.* **12**: 133–156.

Panchang, V. G., W. Ge, B. Cushman-Roisin, and B. R. Pearce (1991). Solution to the mild-slope wave problem by iteration. *Appl. Ocean Res.* **13**(4): 187–199.

Panchang, V. G., B. Xu, and B. Cushman-Roisin (1993). Bathymetric variations in the exterior domain of a harbor wave model. *Proc. Int. Conf. Hydroscience and Eng.* Washington DC. 1555–1562.

Panchang, V. G., B. Xu, and Z. Demirbilek (1999). Wave prediction models for coastal engineering applications. In: *Developments in Offshore Engineering*, ed. J. B. Herbich. Chapter 4. Gulf Publishing, Houston. 163–194.

Panchang, V. G., W. Chen, B. Xu, K. Schlenker, Z. Demirbilek, and M. Okihiro (2000). Effects of exterior bathymetry in elliptic harbor wave models. *J. Waterway, Port, Coastal & Ocean Eng.* **126**(2): 71–78.

Pos, J. D. (1985). Asymmetrical breakwater gap wave diffraction using finite and infinite elements. *Coastal Eng.* **9**: 101–1123.

Pos, J. D. and F. A. Kilner (1987). Breakwater gap wave diffraction: An experimental and numerical study. *J. Waterway, Port, Coastal & Ocean Eng.* **113**(1): 1–21.

Pos, J. D., J. W. Gonsalves, and A. H. Holtzhausen (1989). Short-wave penetration of harbors: A case study at Mossel Bay. *Proc. 9th Ann. Conf. Finite Element Meth.*, February 8–10, Stellenbosch, South Africa.

Porter, D. and D. J. Staziker (1995). Extensions of the mild-slope equation. *J. Fluid Mech.* **300**: 367–382.

Radder, A. C. (1979). On the parabolic equation method for water-wave propagation. *J. Fluid Mech.* **95**: 159–176.

Radder A. C. (1992). Efficient elliptic solvers for the mild-slope equation using the multigrid method. *Coastal Eng.* **18**: 347–352.

Schaffer, H. A. and I. G. Jonsson (1992). Edge waves revisited. *Coastal Eng.* **16**: 349–368.

Seabergh, W. C. and L. J. Thomas (1995). *Los Angeles Harbor Pier 400 Harbor Resonance Model Study.* US Army Corps. of Engineers Waterways Expt. Stn., Vicksburg, MS 39180. TR CERC-95-8.

Smith, G. D. (1978). *Numerical Solution of Partial Differential Equations: Finite Difference Mathods.* Oxford University Press.

Smith, R. and T. Sprinks (1975). Scattering of surface waves by a conical island, *J. Fluid Mech.* **72**: 373.

Steward, D. R. and V. G. Panchang (2000). Improved coastal boundary conditions for water wave simulation models. *Ocean Eng.* **28**: 139–157.

Sutherland, J. and T. O'Donoghue (1998). Wave phase shift at coastal structures. *J. Waterway, Port, Coastal & Ocean Eng.* **124**(2): 80–98

Tang, Y. and Y. Ouellet (1997). A new kind of nonlinear mild-slope equation for combined refraction-diffraction of multifrequency waves. *Coast. Eng.* **31**: 3–36.

Tang, Y., Y. Ouellet, and Y. Ropars (1999). Finite element modeling of wave conditions inside Sainte-Therese-de-gaspe Harbor, Quebec. *Proc. Canadian Coastal Conf.* 737–748.

Thompson, E. F., H. S. Chen, and L. L. Hadley (1996). Validation of numerical model for wind waves and swell in harbors. *J. Waterway, Port, Coastal & Ocean Eng.* **122**(5): 245–256.

Tsay, T.-K. and P. L.-F. Liu (1983). A finite element model for wave refraction and diffraction. *Appl. Ocean Res.* **5**(1): 30–37.

Tsay, T.-K., W. Zhu, and P. L.-F. Liu (1989). A finite-element model for wave refraction, diffraction, reflection, and dissipation. *Appl. Res.* **11**: 33–38.

Whalin, R. W. (1971). *The Limit of Application of Linear Refraction Theory in A Convergence Zone.* US Army Corps. of Engineers Waterways Experiment Station, Vicksburg. Research Rept H-71-3.

Xu, B. and V. G. Panchang (1993). Outgoing boundary conditions for elliptic water wave models. *Proc. R. Soc. London, Ser. A* **441**: 575–588.

Xu, B., V. G. Panchang, and Z. Demirbilek (1996). Exterior reflections in elliptic harbor wave models. *J. Waterway, Port, Coastal & Ocean Eng.* **122**(3): 118–126.

YOTO (1998). "Our Ocean Future", Year of the Ocean, Themes & Issues Concerning the Nation's Stake in the Oceans. Prepared by the H. John Heinz III Center for Science, Economics, and the Environment. Office of the Chief Scientist, NOAA, Washington, DC 20230.

Zhao, L., V. G. Panchang, W. Chen, Z. Demirbilek, and N. Chhabbra (2000). Simulation of breaking effects in a two-dimensional harbor wave prediction model. *Coastal Eng.* To appear.

Zundell, A. K., A. L. Fugal, N. L. Jones, and Z. Demirbilek (1998). Automatic definition of two-dimensional coastal finite element domains. In: *Hydroinformatics98, Proc. 3rd Int. Conf. Hydroinformatics.* eds. V. Babovic and L. C. Larsen. A. A. Balkema, Rotterdam. 693–700.

RECENT ADVANCES IN THE MODELING OF WAVE AND PERMEABLE STRUCTURE INTERACTION

INIGO J. LOSADA

Artificial and natural porous structures are of great interest in coastal and harbor engineering. The modeling of wave interaction with permeable structures is therefore a key issue to determine the functionality and stability of this kind of structures. In most circumstances, an averaging process is introduced in the analysis of the flow in terms of a seepage or discharge velocity and some coefficients depending on the flow. In order to solve the wave and structure interaction, the porous flow model is matched with a flow model for the fluid region. In this paper, it will be shown that several new equations including the resistance forces in the porous medium have been derived. Newly developed models based on Boussinesq-type equations or direct resolution of the Navier–Stokes equations using VOF techniques have opened a new range of possible applications. However, these models still highly depend on porous flow coefficients. Predictive formulae for these constants under oscillatory flow conditions require further research especially if these models are considered to be an alternative to physical modeling in the design of coastal structures.

1. Introduction

A porous medium is a two-phase material in which the solid matrix, usually assumed to be rigid, constitutes one phase and the interconnected voids or pores constitutes the other. One of the main characteristics of porous media is the irregular shape and size of its pores, randomly distributed, conferring the flow through this heterogeneous formation considered a very complex nature. Our interest will be to determine the flow through the porous formation with typical length scales much larger than the characteristic pore size.

Artificial porous structures such as rubble-mound breakwaters, submerged structures, outfall protections, artificial fishing reefs or armor layers for the protection of seawalls or vertical structures are of great interest in coastal and harbor engineering since they provide one of the best means to induce incident wave dissipation by friction inside the structures. Therefore, the knowledge